Biological Imaging

DOI: 10.1002/anie.200801810

Micellar Hybrid Nanoparticles for Simultaneous Magnetofluorescent Imaging and Drug Delivery**

*Ji-Ho Park, Geoffrey von Maltzahn, Erkki Ruoslahti, Sangeeta N. Bhatia, and Michael J. Sailor**

Multifunctional nanoparticles have the potential to integrate therapeutic and diagnostic functions into a single nanodevice.[1–9] To date, several types of hybrid nanosystems containing various types of nanoparticles have been developed that allow multimodal imaging. For example, formulations containing quantum dots (QDs) and magnetic iron oxide nanoparticles (MNs) provide a means to perform simultaneous fluorescence optical imaging and magnetic resonance imaging (MRI).[10–15] Although these nanocomposites have been used for in vitro magnetic cell separation and in vitro cell targeting, in vivo studies, in particular for cancer imaging and therapy, have been limited owing to the poor stability or short systemic circulation times generally observed for these more complicated nanostructures.[16,17] Herein, we describe long-circulating, micellar hybrid nanoparticles (MHNs) that contain MNs, QDs, and the anticancer drug doxorubicin (DOX) within a single poly(ethylene glycol) (PEG)–phospholipid micelle and provide the first examples of simultaneous targeted drug delivery and dual-mode near-infrared (NIR) fluorescence imaging and MRI of diseased tissue in vitro and in vivo.

Micellar preparations of hydrophobic drugs and nanoparticles coated with diblock polymers hold great potential for biomedical applications.[18–24] Such micellar coatings often display excellent stability and thus decrease the cytotoxicity of the hydrophobic drug or nanoparticle contents. Previous in vitro studies have demonstrated that drug molecules and MNs can be incorporated within a micelle to enable the corroboration of drug delivery by MRI.[21,23] Furthermore, micellar preparations containing single-component nanomaterials, such as QDs and carbon nanotubes, have been shown to be sufficiently stable for in vivo applications.[18,24]

Our synthesis of MHNs is derived from a previously reported method for the micellar encapsulation of QDs.[18] Briefly, spherical oleic acid coated MNs with a diameter of 11 nm and elongated trioctylphosphine-coated QDs with a longitudinal size of 10–12 nm and an NIR emission wavelength were encapsulated simultaneously within micelles composed of a PEG-modified phospholipid (Figure 1). The

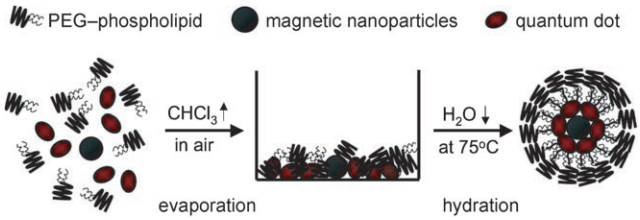

Figure 1. Synthetic procedure used to prepare micellar hybrid nanoparticles that encapsulate magnetic nanoparticles and quantum dots within a single PEG-modified phopholipid micelle.

MHNs were removed from the micellar MNs (MMNs), micellar QDs (MQDs), and empty micelle by-products by magnetic separation and centrifugation. Transmission electron microscope images and dynamic light scattering measurements revealed that the MHNs consist of clusters of both MNs and QDs within a micellar coating with a hydrodynamic size of 60–70 nm (Figure 2a–d). The MN/QD ratio within the individual micelles could be adjusted by changing the mass ratio of MNs to QDs during the synthesis. By contrast, MMNs and MQDs prepared by encapsulating MNs or QDs alone with PEG–phospholipids appeared to be individually encapsulated and encapsulated as dimers, respectively (Figure 2e,f). When relatively concentrated solutions of MNs and QDs ($>2\,mg\,mL^{-1}$) were added to the PEG–phospholipid solution during micelle formation, aggregates rather than isolated nanoparticles formed. All preparations that produced MHNs in a concentration of approximately $1\,mg\,mL^{-1}$ were stable in deionized water or phosphate buffered saline (PBS), with no observable aggregation or dissociation for at least 1 month. Unlike the dispersed arrangements of MNs and QDs reported for previous hybrid systems,[13,14] the MNs and QDs in the MHNs appear to be closely packed within a single micelle in a way that

[*] J.-H. Park, Prof. M. J. Sailor
Materials Science and Engineering Program
Department of Chemistry and Biochemistry
University of California, San Diego
9500 Gilman, La Jolla, CA 92093 (USA)
E-mail: msailor@ucsd.edu
G. von Maltzahn, Prof. S. N. Bhatia
Harvard-MIT Division of Health Sciences and Technology
Massachusetts Institute of Technology
77 Massachusetts Avenue, Cambridge, MA 02139 (USA)
Prof. E. Ruoslahti
Burnham Institute for Medical Research at UCSB
University of California, Santa Barbara
1105 Life Sciences Technology Bldg, Santa Barbara, CA 93106 (USA)

[**] This project was funded in part with federal funds from the National Cancer Institute of the National Institutes of Health (Contract No. R01A124427-02 and U01 HL 080718). M.J.S., E.R., and S.N.B. are members of the Moores UCSD Cancer Center and the UCSD NanoTUMOR Center, under the auspices of which this research was conducted and partially supported through an NIH Grant (U54 CA 119335). J.P. thanks the Korea Science and Engineering Foundation (KOSEF) for a Graduate Study Abroad Scholarship. We thank Dr. Edward Monosov for assistance with TEM analysis.

Supporting information for this article is available on the WWW under http://dx.doi.org/10.1002/anie.200801810.

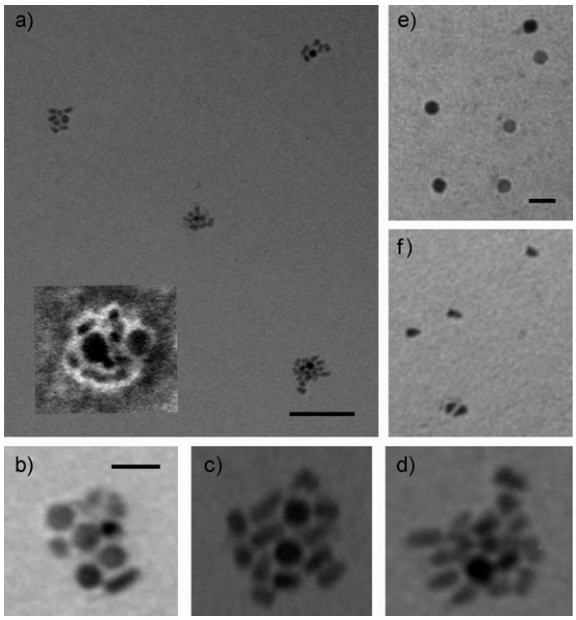

Figure 2. a) Transmission electron microscope (TEM) image (scale bar: 100 nm) of micellar hybrid nanoparticles (MHNs) with an MN/QD mass ratio of 1:5. (Inset: TEM image of an individual MHN following treatment with a 1.3% phosphotungstic acid negative stain. The brighter regions are associated with the micellar coating). b–d) Magnified TEM images (scale bar: 20 nm) of MHNs with an MN/QD mass ratio of 1:1 (MHN1, b), 1:3 (MHN3, c), and 1:5 (MHN5, d). e) TEM image (scale bar: 20 nm) of micellar magnetic nanoparticles. f) TEM image (scale bar: 20 nm) of micellar quantum dots (λ_{max}(emission) = 705 nm). In these formulations, the QDs have an elongated shape (2:1 aspect), and the MNs are spherical.

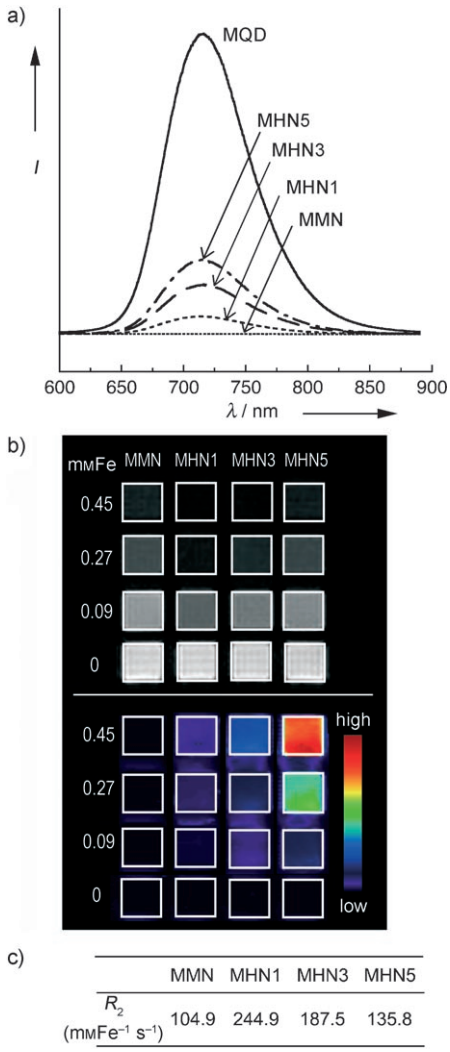

Figure 3. a) Photoluminescence spectra of micellar quantum dots (MQDs, λ_{max}(emission) = 705 nm), micellar magnetic nanoparticles (MMNs), and micellar hybrid nanoparticles (MHNs) containing MNs and QDs in different ratios. The particle samples were excited with light at 450 nm. The intensity (I) of each spectrum was normalized on the basis of the total mass of each particle type. b) Multimodal imaging of MMNs and MHNs as a function of iron concentration by MRI (top, T_2-weighted mode) and NIR fluorescence (bottom, in the Cy5.5 fluorescence channel, λ_{ex} = 680 nm, λ_{obs} = 720 nm). c) Relaxivity R_2 values of the MMNs and MHNs in the T_2-weighted magnetic resonance images.

resembles the clustering of MNs that has been observed inside poly(caprolactone)–PEG copolymer systems.[22]

To examine the possibility of the remote imaging of the MHN preparations, fluorescence spectra were measured with excitation in the blue (450 nm) and NIR (680 nm) regions (Figure 3). In both cases, as the ratio of MNs to QDs within a micelle increased, the intensity of fluorescence from the MHN assembly decreased with no significant spectral shift or line broadening of the emission spectrum observed. The loss of fluorescence intensity can be attributed to a decreased number of QDs per micelle and to optical absorption by the MNs and is consistent with previous observations.[13,14] Additionally, the proximity of MNs and other QDs in the MHNs is likely to cause fluorescence quenching through nonradiative energy or charge transfer.[10,25] Despite quenching, fluorescence is intense enough to enable the detection of MHNs at subnanomolar QD concentrations. These inorganic QD-containing hybrid systems can be excited and observed in the NIR spectral region with high photostability,[26,27] a property that provides significant advantages over MNs labeled with organic fluorophores.[28,29]

The MHN materials can also be imaged with MRI. The MR characteristics of MHNs with varying MN/QD ratios were compared to those of MMNs (Figure 3b,c). The T_2-weighted images of MHN1 and MHN3, which contain MN clusters, display significantly larger MR contrast than those of MMN, which contains only a single MN (T_2 relaxation rates: R_2 = 244.9 (MHN1), 187.5 (MHN3), 104.9 mM Fe^{-1} s^{-1} (MMN)). The increased T_2 relaxivity for coalesced MNs has been observed in several previous studies[2,22,30] and highlights an unexpected benefit of coencapsulating both materials; this effect is not observed for nanohybrids that contain a single MN.[5,28,31,32] SQUID (superconducting quantum interference device) magnetic measurements confirm that MHNs retain the superparamagnetic characteristics of individual MNs (see the Supporting Information, Figure S1). The MHNs are thus detectable by both MRI and fluorescence at submicromolar Fe and subnanomolar QD concentrations (Figure 3b), which highlights their utility for bimodal applications.

The ability of MHNs to target and dual-mode image tumor cells was tested on MDA-MB-435 human cancer cells. To enable the specific targeting of tumor cells by the nanoassemblies, the MHNs were conjugated with the targeting ligand F3, a peptide known to target cell-surface nucleolin in endothelial cells in tumor blood vessels and in tumor cells and to become internalized in these cells.[33,34] This peptide is capable of transporting payloads, such as nanoparticles or oligonucleotides, into tumor vasculature in vivo.[35–37] Cells incubated with F3-conjugated MHNs (F3-MHNs) displayed dramatically increased NIR fluorescence and MRI contrast, whereas cells incubated with unmodified MHNs exhibited no significant fluorescence or MRI contrast (Figure 4a,b).

Simultaneous imaging and drug delivery was demonstrated with the anticancer drug doxorubicin (DOX), which was incorporated into the MHNs during synthesis (DOX/MHN ≈ 0.093:1 (w/w); see the Supporting Information, Figure S2). The intrinsic fluorescence of DOX enabled the independent imaging of both DOX and QDs contained in the MHNs. The intact MHNs were observed to colocalize in some areas of MDA-MB-435 cells in vitro upon incubation for 2 h (Figure 4c). During a 24 h period, F3-MHNs were observed to chaperone DOX into cancer cells and release it endosomally into the nuclei following tumor-cell internalization (inset in Figure 4c; see the Supporting Information, Figure S3). After incubation for 30 min with DOX-loaded F3-MHNs (DOX-MHN-F3), the DOX fluorescence signal appeared mainly in the cytoplasm and showed the colocalization of DOX with endosomes. In contrast, when free DOX was added, almost all of the DOX fluorescence signal was observed in the cell nuclei. As the incubation time increased, the DOX in the cytoplasm was observed to translocate into the nuclei.

Although they are composed of relatively toxic QDs, no significant toxicity of the MHN assemblies was observed in this study, a result consistent with those of previous in vitro and in vivo studies with MQDs and liposomal hybrid particles containing QDs and MNs.[17,18] By contrast, F3-MHNs in which DOX was incorporated displayed significantly greater cytotoxicity than that of equivalent quantities of free DOX or MHNs containing DOX without the targeting ligand (see the Supporting Information, Figure S4).

We next investigated the utility of MHNs for multimodal in vivo imaging applications. We synthesized MHNs that contain QDs and emit at a wavelength of 800 nm (MHN-(800)). This NIR wavelength is appropriate for the imaging of organs in vivo and ex vivo because it maximizes tissue penetration while minimizing optical absorption by physiologically abundant species, such as hemoglobin (see the Supporting Information, Figure S5).[38] These PEG-coated MHNs exhibited substantial blood-circulation times ($t_{1/2}$ = 3 h) comparable to those of other PEG–nanomaterial formulations ($t_{1/2}$ = 0.5–2 h for PEGylated carbon nanotubes, $t_{1/2}$ = 0.2–2.2 h for PEGylated QDs).[24,39,40] We confirmed that MHNs survive circulation in the blood stream without dissociation into individual MNs or QDs by transmission electron microscopy (see the Supporting Information, Figure S6a).

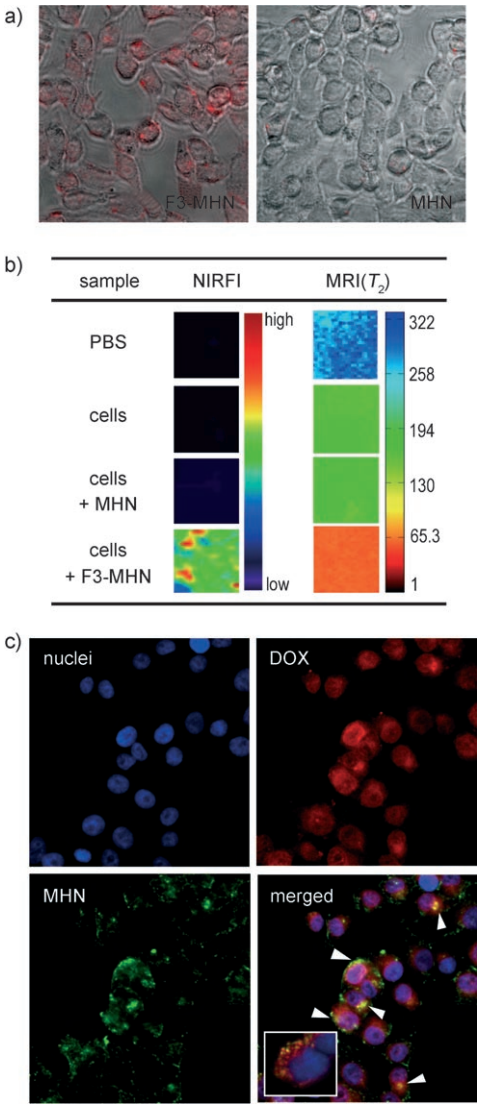

Figure 4. a) Intracellular delivery of F3-conjugated micellar hybrid nanoparticles (F3-MHNs) into MDA-MB-435 human carcinoma cells. The F3-MHN particles and the MHN control particles appear red in the images. After incubation for 2 h with the cells, the F3-MHN particles were strongly associated with the cells, whereas the control MHN nanoparticles without the F3 ligand did not penetrate. b) Multimodal images (NIR fluorescence in the Cy5.5 channel and MRI) of the cells in (a), a PBS control, and untreated cells. c) Targeted drug delivery of F3-MHNs containing DOX into MDA-MB-435 human carcinoma cells. The DOX-loaded F3-MHNs were incubated with the cells for 2 h. Arrowheads indicate colocalization of DOX and MHNs. The inset shows the colocalization of some DOX (red) and the endosome marker (green) 30 min after incubation with DOX-loaded F3-MHNs. The nuclei were stained with 4′-6-diamidino-2-phenylindole (DAPI).

Long-circulating nanoparticles in the size range of 20–200 nm have been shown to accumulate preferentially at tumor sites through an enhanced permeability and retention effect.[41,42] Nude mice with MDA-MB-435 tumors were imaged prior to injection of the MHNs and then 20 h after injection. In these optical images, significant fluorescence was observed in the tumors 20 h after injection of the MHNs (Figure 5a). Biodistribution measurements indicated that

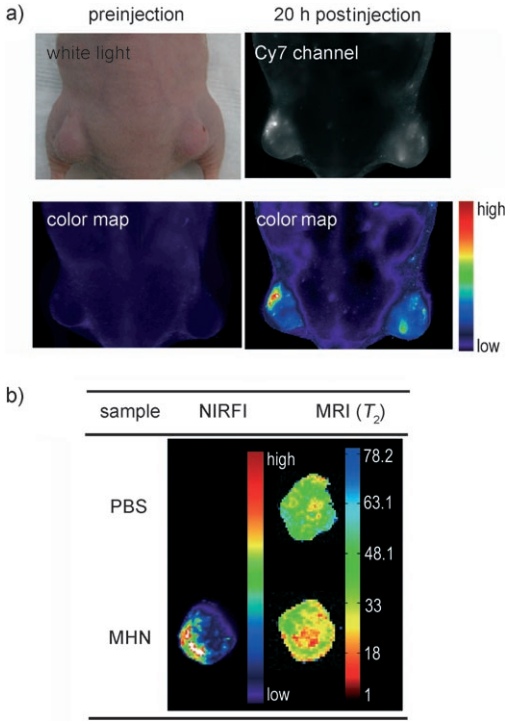

Figure 5. a) NIR fluorescence images showing the passive accumulation of MHNs containing QDs (emission at 800 nm, MHN(800)) in a mouse with MDA-MB-435 tumors. The mouse was imaged preinjection and 20 h postinjection (injection dose: 10 mg kg^{-1}). b) Image table describing the results of multimodal imaging (by MRI and NIR fluorescence) of the tumor harvested from the mouse in (a). PBS: a control in which a mouse with a tumor was injected with phosphate buffered saline; NIRFI: near-infrared fluorescence image; MRI(T_2): T_2 values from T_2-weighted MRI.

MHNs accumulate mainly in the liver; the quantity of MHNs observed in other organs was not significant (see the Supporting Information, Figure S6b). To evaluate the efficacy of combined MR and optical imaging, the tumors were harvested 20 h after injection and imaged immediately with a 4.7 T MRI scanner and with a NIR optical-imaging system. Significant differences in both fluorescence and MRI contrast were observed between tumors injected with PBS and those injected with MHNs (Figure 5b; see the Supporting Information, Figure S6c). The differences observed in the fluorescence images are much more substantial than those observed in the MR images as a result of the low background signals associated with NIR imaging. Although these in vivo results are preliminary, the data suggest that the method is promising for further in vivo applications owing to the prolonged residence time in blood circulation displayed by MHNs relative to that of similar liposomal hybrid systems.[17]

In summary, micellar hybrid nanoparticles that contain MNs, QDs, and the anticancer drug DOX within a single PEG-modified phospholipid micelle have been prepared. The strong interaction of the hydrophobic chains of the PEG–phospholipids with hydrophobic chains attached to the MNs and QDs leads to high dispersibility and stability for in vitro and in vivo applications. The MHNs enable dual-mode imaging of cells in vitro and organs in vivo or ex vivo, whereby the advantages of optical imaging (for microscopic resolution and in vivo fluorescence imaging) and MRI (for the determination of full anatomical distribution in vivo) are combined. This approach may be applicable to the synthesis of other hybrid nanodevices that combine the dissimilar functions of two or more nanomaterials, for example, properties appropriate for MRI, photothermal therapy, Raman imaging, and fluorescence imaging. Simultaneous dual-mode diagnosis and therapy with the hybrid system reported herein may enable more effective early detection and treatment of various types of cancer.

Received: April 17, 2008
Revised: July 1, 2008
Published online: August 11, 2008

Keywords: antitumor agents · drug delivery · magnetic nanoparticles · micelles · quantum dots

[1] T. J. Harris, G. von Maltzahn, A. M. Derfus, E. Ruoslahti, S. N. Bhatia, *Angew. Chem.* **2006**, *118*, 3233 – 3237; *Angew. Chem. Int. Ed.* **2006**, *45*, 3161 – 3165.
[2] J.-H. Lee, Y.-w. Jun, S.-I. Yeon, J.-S. Shin, J. Cheon, *Angew. Chem.* **2006**, *118*, 8340 – 8342; *Angew. Chem. Int. Ed.* **2006**, *45*, 8160 – 8162.
[3] J. Kim, S. Park, J. E. Lee, S. M. Jin, J. H. Lee, I. S. Lee, I. Yang, J.-S. Kim, S. K. Kim, M.-H. Cho, T. Hyeon, *Angew. Chem.* **2006**, *118*, 7918 – 7922; *Angew. Chem. Int. Ed.* **2006**, *45*, 7754 – 7758.
[4] W. J. M. Mulder, R. Koole, R. J. Brandwijk, G. Storm, P. T. K. Chin, G. J. Strijkers, C. de Mello Donegá, K. Nicolay, A. W. Griffioen, *Nano Lett.* **2006**, *6*, 1 – 6.
[5] C. Xu, J. Xie, D. Ho, C. Wang, N. Kohler, E. G. Walsh, J. R. Morgan, Y. E. Chin, S. Sun, *Angew. Chem.* **2008**, *120*, 179 – 182; *Angew. Chem. Int. Ed.* **2008**, *47*, 173 – 176.
[6] X. Zhang, M. Brynda, R. D. Britt, E. C. Carroll, D. S. Larsen, A. Y. Louie, S. M. Kauzlarich, *J. Am. Chem. Soc.* **2007**, *129*, 10668 – 10669.
[7] A. M. Derfus, G. von Maltzahn, T. J. Harris, T. Duza, K. S. Vecchio, E. Ruoslahti, S. N. Bhatia, *Adv. Mater.* **2007**, *19*, 3932 – 3936.
[8] Y.-M. Huh, E.-S. Lee, J.-H. Lee, Y.-w. Jun, P.-H. Kim, C.-O. Yun, J.-H. Kim, J.-S. Suh, J. Cheon, *Adv. Mater.* **2007**, *19*, 3109 – 3112.
[9] J. H. Choi, F. T. Nguyen, P. W. Barone, D. A. Heller, A. E. Moll, D. Patel, S. A. Boppart, M. S. Strano, *Nano Lett.* **2007**, *7*, 861 – 867.
[10] D. Wang, J. He, N. Rosenzweig, Z. Rosenzweig, *Nano Lett.* **2004**, *4*, 409 – 413.
[11] D. K. Yi, S. T. Selvan, S. S. Lee, G. C. Papaefthymiou, D. Kundaliya, J. Y. Ying, *J. Am. Chem. Soc.* **2005**, *127*, 4990 – 4991.
[12] J. Kim, J. E. Lee, J. Lee, J. H. Yu, B. C. Kim, K. An, Y. Hwang, C.-H. Shin, J.-G. Park, J. Kim, T. Hyeon, *J. Am. Chem. Soc.* **2006**, *128*, 688 – 689.
[13] T. R. Sathe, A. Agrawal, S. Nie, *Anal. Chem.* **2006**, *78*, 5627 – 5632.
[14] B.-S. Kim, T. A. Taton, *Langmuir* **2007**, *23*, 2198 – 2202.
[15] E.-Q. Song, G.-P. Wang, H.-Y. Xie, Z.-L. Zhang, J. Hu, J. Peng, D.-C. Wu, Y.-B. Shi, D.-W. Pang, *Clin. Chem.* **2007**, *53*, 2177 – 2185.
[16] B. Zebli, A. S. Susha, G. B. Sukhorukov, A. L. Rogach, W. J. Parak, *Langmuir* **2005**, *21*, 4262 – 4265.
[17] G. Beaune, B. Dubertret, O. Clement, C. Vayssettes, V. Cabuil, C. Menager, *Angew. Chem.* **2007**, *119*, 5517 – 5520; *Angew. Chem. Int. Ed.* **2007**, *46*, 5421 – 5424.

[18] B. Dubertret, P. Skourides, D. J. Norris, V. Noireaux, A. H. Brivanlou, A. Libchaber, *Science* **2002**, *298*, 1759 – 1762.
[19] Z. Gao, A. N. Lukyanov, A. Singhal, V. P. Torchilin, *Nano Lett.* **2002**, *2*, 979 – 982.
[20] V. P. Torchilin, A. N. Lukyanov, Z. Gao, B. Papahadjopoulos-Sternberg, *Proc. Natl. Acad. Sci. USA* **2003**, *100*, 6039 – 6044.
[21] T. K. Jain, M. A. Morales, S. K. Sahoo, D. L. Leslie-Pelecky, V. Labhasetwar, *Mol. Pharm.* **2005**, *2*, 194 – 205.
[22] H. Ai, C. Flask, B. Weinberg, X. Shuai, M. D. Pagel, D. Farrell, J. Duerk, J. Gao, *Adv. Mater.* **2005**, *17*, 1949 – 1952.
[23] N. Nasongkla, E. Bey, J. Ren, H. Ai, C. Khemtong, J. S. Guthi, S.-F. Chin, A. D. Sherry, D. A. Boothman, J. Gao, *Nano Lett.* **2006**, *6*, 2427 – 2430.
[24] Z. Liu, W. B. Cai, L. N. He, N. Nakayama, K. Chen, X. M. Sun, X. Y. Chen, H. J. Dai, *Nat. Nanotechnol.* **2007**, *2*, 47 – 52.
[25] S. K. Mandal, N. Lequeux, B. Rotenberg, M. Tramier, J. Fattaccioli, J. Bibette, B. Dubertret, *Langmuir* **2005**, *21*, 4175 – 4179.
[26] I. L. Medintz, H. T. Uyeda, E. R. Goldman, H. Mattoussi, *Nat. Mater.* **2005**, *4*, 435 – 446.
[27] X. Michalet, F. F. Pinaud, L. A. Bentolila, J. M. Tsay, S. Doose, J. J. Li, G. Sundaresan, A. M. Wu, S. S. Gambhir, S. Weiss, *Science* **2005**, *307*, 538 – 544.
[28] L. Josephson, M. F. Kircher, U. Mahmood, Y. Tang, R. Weissleder, *Bioconjugate Chem.* **2002**, *13*, 554 – 560.
[29] R. Weissleder, K. Kelly, E. Y. Sun, T. Shtatland, L. Josephson, *Nat. Biotechnol.* **2005**, *23*, 1418 – 1423.
[30] J. M. Perez, L. Josephson, T. O'Loughlin, D. Högemann, R. Weissleder, *Nat. Biotechnol.* **2002**, *20*, 816 – 820.
[31] J.-S. Choi, Y.-W. Jun, S.-I. Yeon, H. C. Kim, J.-S. Shin, J. Cheon, *J. Am. Chem. Soc.* **2006**, *128*, 15982 – 15983.
[32] H. Gu, R. Zheng, X. Zhang, B. Xu, *J. Am. Chem. Soc.* **2004**, *126*, 5664 – 5665.
[33] K. Porkka, P. Laakkonen, J. A. Hoffman, M. Bernasconi, E. Ruoslahti, *Proc. Natl. Acad. Sci. USA* **2002**, *99*, 7444 – 7449.
[34] S. Christian, J. Pilch, M. E. Akerman, K. Porkka, P. Laakkonen, E. Ruoslahti, *J. Cell Biol.* **2003**, *163*, 871 – 878.
[35] M. E. Akerman, W. C. W. Chan, P. Laakkonen, S. N. Bhatia, E. Ruoslahti, *Proc. Natl. Acad. Sci. USA* **2002**, *99*, 12617 – 12621.
[36] G. R. Reddy, M. S. Bhojani, P. McConville, J. Moody, B. A. Moffat, D. E. Hall, G. Kim, Y.-E. L. Koo, M. J. Woolliscroft, J. V. Sugai, T. D. Johnson, M. A. Philbert, R. Kopelman, A. Rehemtulla, B. D. Ross, *Clin. Cancer Res.* **2006**, *12*, 6677 – 6686.
[37] E. Henke, J. Perk, J. Vider, P. de Candia, Y. Chin, D. B. Solit, V. Ponomarev, L. Cartegni, K. Manova, N. Rosen, R. Benezra, *Nat. Biotechnol.* **2008**, *26*, 91 – 100.
[38] R. Weissleder, *Nat. Biotechnol.* **2001**, *19*, 316 – 317.
[39] A. N. Lukyanov, Z. Gao, L. Mazzola, V. P. Torchilin, *Pharm. Res.* **2002**, *19*, 1424 – 1429.
[40] B. Ballou, B. C. Lagerholm, L. A. Ernst, M. P. Bruchez, A. S. Waggoner, *Bioconjugate Chem.* **2004**, *15*, 79 – 86.
[41] R. K. Jain, *Annu. Rev. Biomed. Eng.* **1999**, *1*, 241 – 263.
[42] H. Maeda, J. Wu, T. Sawa, Y. Matsumura, K. Hori, *J. Controlled Release* **2000**, *65*, 271 – 284.

